Photo-Rechargeable Zinc-Ion Capacitors using V_2O_5 – Activated Carbon Electrodes

Buddha Deka Boruah[1,], Bo Wen[1,2], Satyawan Nagane[3], Xiao Zhang[1], Samuel D. Stranks[3], Adam Boies[1], Michael De Volder[1,*]*

[1]Department of Engineering, University of Cambridge, Cambridge CB3 0FS, United Kingdom

[2]Cambridge Graphene Centre, University of Cambridge, Cambridge CB3 0FA, United Kingdom

[3]Cavendish Laboratory, University of Cambridge, JJ Thomson Ave, Cambridge CB3 0HE, United Kingdom

* Corresponding authors. E-mail: bd411@cam.ac.uk

mfld2@cam.ac.uk

Abstract

Electrochemical energy storage devices that can harvest energy from the environment and store it are increasingly important to address both energy poverty in developing parts of the world, as well as powering off-grid autonomous devices. Currently, batteries or supercapacitors connected to solar cells are used for these applications, but these frequently suffer from voltage mismatches and inefficiencies in the device packaging. This paper presents an optically and electrochemically active electrode for photo-rechargeable zinc-ion capacitors using vanadium oxide nanofibers. These rely on photo-excited charge carrier separation to charge the capacitors without any external photovoltaic or electrical devices. We found that silver nanowires are better than carbon based conductive additives as they support photo-excited holes transport and provides light scattering centers that enhance visible light absorption. The proposed capacitors show a ~ 63% capacity increase under illumination, photo-recharge in 30 minutes and ~ 99% capacity retention over 4000 cycles.

Table of Content (TOC) Graphic

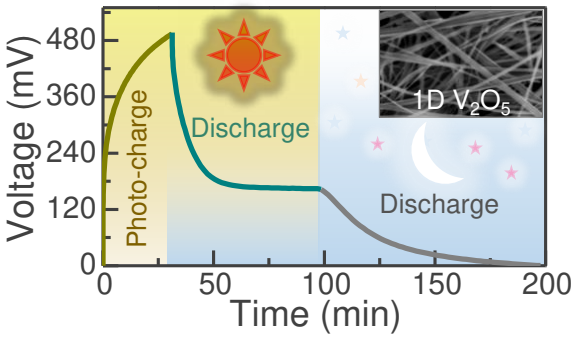

To date, many communities in developing countries still lack access to environmentally benign and cost-effective energy solutions. This energy poverty is a grand challenge for off-grid communities for which few viable energy sources are available. The most commonl solution is to combine photovoltaic devices with batteries or electrochemical capacitors.[1-5] A number of academic papers have looked into integrating these devices efficiently. For instance, Hui *et al.* proposed a portable and efficient solar-rechargeable battery system based on a perovskite solar module integrated with an aluminum ion battery;[6] Xu *et al.* reported a lithium-ion battery (LIB) integrated with perovskite solar cells;[7] Liu and co-workers considered polypyrrole-based supercapacitors recharged by silicon nanowire/polymer hybrid solar cell.[8] However, integrated energy harvesting and storing devices introduce some challenges in device packaging efficiency and ohmic transport losses.[9,10] Further, the output voltage of photovoltaic cells is often insufficient to fully charge the batteries or capacitors, which then requires additional electronics that add to the cost of the devices.[7,10-12]

Recently, there have been some developments towards electrodes of batteries and capacitors that can directly harvest solar power without the need for solar cells, thereby offering an elegant solution for the challenges listed above.[10,13-19] Here we present a new light rechargeable electrochemical capacitors. In general, electrochemical supercacacitors have drawn attention in the scientific community because of their high power density, fast charge, long cycling life and safe operation.[20] However, they suffer from low energy density, and to bridge the gap in power density and energy density between supercapacitors and LIBs, a new class of energy storage devices known as metal ion capacitors have been proposed.[21,22] Recently, aqueous zinc-ion capacitors (ZICs) have been studied because of their environmental friendliness and low cost compared to non-aqueous lithium or sodium ion capacitors.[23,24]

Recently, a photo-rechargeable ZIC (hν-ZIC) was proposed using graphitic carbon nitride as the active material.[25] This system achieved a light conversion efficiencies of ~ 0.01%, photo-charge energy densities of 0.7 Wh kg^{-1} and photo-charge capacities of 11.4 F g^{-1}.[25] Here, we report an improved hν-ZIC system using vanadium pentoxide (V_2O_5) based photoanodes with activated carbon (AC) cathodes as illustrated in **Figure 1a** (the photo-charging mechanism is discussed further on). V_2O_5 is selected here because of its bandgap in the visible light spectrum and its ability to reversibly intercalate/deintercalate Zn ions (see further). The energy band alignment of the photoanodes is studied using chirality sorted (6,5) semi-conducting single walled carbon nanotubes (SCNTs), conducting multi walled carbon nanotubes (MCNTs) and silver (Ag) nanowires. These electrodes allow for light charging without external circuit, with the best photo conversion efficiency achieved for the Ag@V_2O_5 system (~ 0.05%). The photo-charge energy density is improved from ~ 0.7 Wh kg^{-1} to ~ 4.8 Wh kg^{-1} and the capacity from ~ 11.4 F g^{-1} to ~ 138 F g^{-1} compared to previous hν-ZICs [25] (these are improvements of 7 and 12 fold respectively). Finally, energy densities of ~ 53 Wh kg^{-1} are achieved, which is comparable to state of the art asymmetric supercapacitors, and the devices achieved stable cycling (4000 cycles) both in dark and light conditions.

One dimensional V_2O_5 nanofibers are explored to improve the charge generation throughout the material and to allow efficient photo-charge conduction along the nanofiber length.[26] These nanofibres are synthesized via a hydrothermal process (see experimental section). **Figure 1b, c** show an SEM image and EDS mapping of the V_2O_5 fibers, which have typical diameters of 20 – 150 nm (a representative EDS spectrum is provided in **Figure 1d**). The high-resolution TEM inset in **Figure 1b** shows an interplanar spacing of ~ 0.34 nm that corresponds to (110) planes of orthorhombic V_2O_5 crystals which is confirmed by XRD in **Figure 1e** (space group: Pmmn (59); JCPDS card no: 03-065-0131). Moreover, Raman spectrum (**Figure S1**) shows characteristic peaks of V_2O_5 which are discussed in supporting information. UV-Vis analysis

in **Figure 1f** shows the V_2O_5 nanofibers have a band edge of ~ 564 nm (~ 2.2 eV, the inset shows the first derivative of absorbance with respect to energy *vs* energy plot).[26,27]

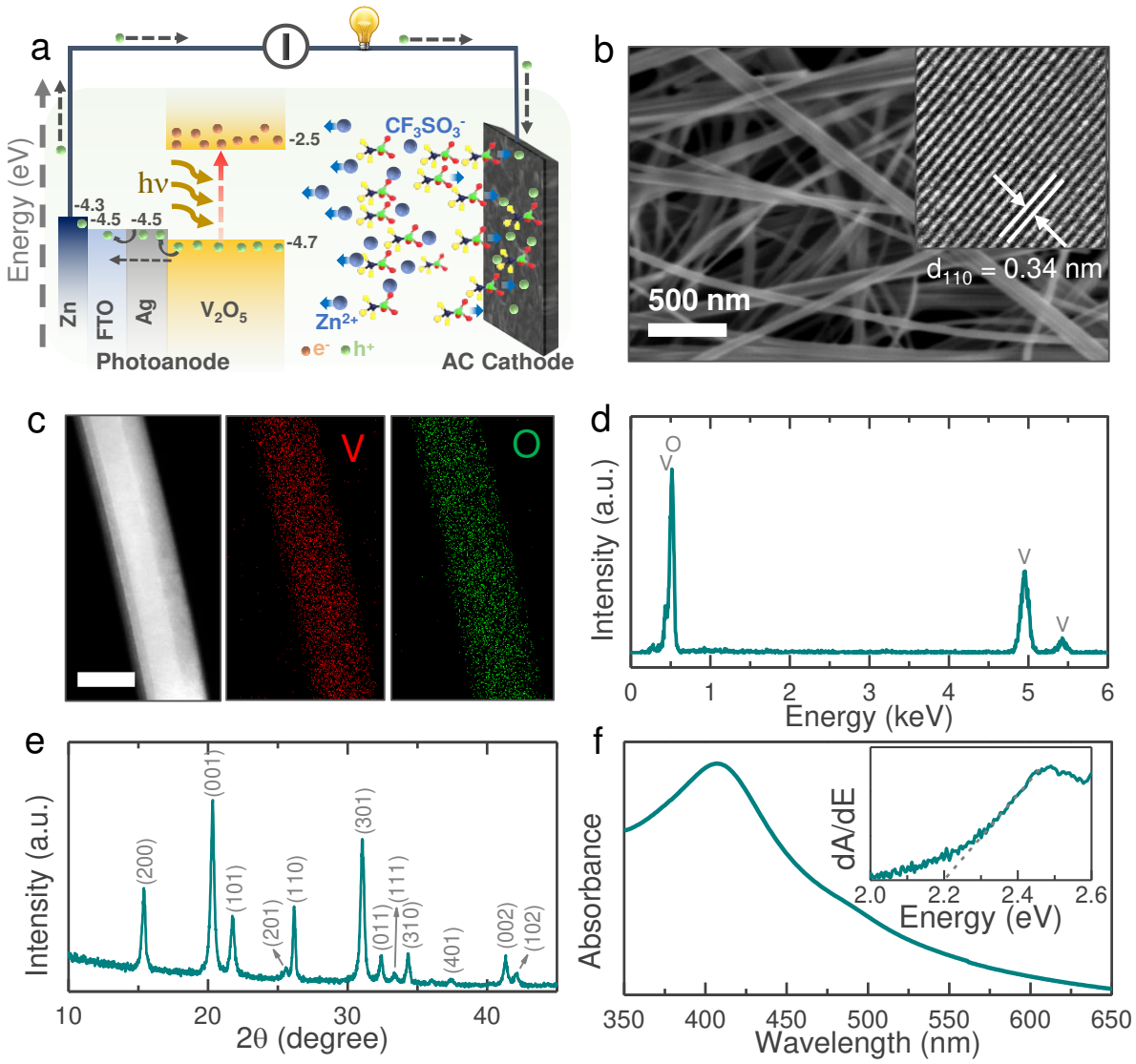

Figure 1. *(a) Schematic representation of hv-ZICs using Ag@V_2O_5 photoanodes and AC cathodes. (b) SEM and TEM (inset) image of V_2O_5 nanofibers. (c,d) Elemental mappings and EDS spectrum of a single nanofiber. Scale bar: 50 nm. (e) XRD pattern of V_2O_5 nanofibers (space group: Pmmn (59); JCPDS card no: 03-065-0131). (f) Absorption spectrum (inset shows the first derivative of absorbance with respect energy vs energy plot).*

The photoanodes are fabricated by mixing same wt% loading of SCNTs, MCNTs or Ag nanowires (see experimental section, **Figure S2a-c** show SEM images) with V_2O_5 nanofibers (these will be referred to as SCNTs@V_2O_5, MCNTs@V_2O_5 and Ag@V_2O_5, respectively). First, to understand the dynamics of the photo-charge carriers, we measure electrical photo-responses of the pristine V_2O_5, SCNTs@V_2O_5, MCNTs@V_2O_5 and Ag@V_2O_5 materials by coating the material on photodetectors using gold (Au) interdigitated electrodes (IDEs, see experimental section). The same amount of photoanode material is drop casted on each Au IDEs followed by current-voltage (IV) measurements shown in **Figure 2a** for Ag@V_2O_5 (IV responses of V_2O_5, SCNTs@V_2O_5 and MCNTs@V_2O_5 are shown in **Figure S3**). The current responses of the photodetectors increase when exposed to light ($\lambda \sim 455$ nm) due to the V_2O_5 nanofibers. The current enhancements ($\frac{I_{ph}-I_d}{I_d} \times 100\%$; where I_d and I_{ph} are current densities in dark and illuminated conditions) of the photodetectors at different bias voltages are shown in **Figure 2b**. The high current enhancement of Ag@V_2O_5 photodetectors (~ 31.9% at 1V) is probably due to the presence of multiple light scattering centers from the Ag nanowires, which increases light interaction probabilities with V_2O_5 (see further).[28-30] However, lower current enhancements of ~ 12.3% and ~ 1.4% at 1 V of the SCNTs@V_2O_5 and MCNTs@V_2O_5 photodetectors as compared to pristine V_2O_5 photodetector (~ 18.9% at 1 V) could be due to the absorption of light by SCNTs and MCNTs (these do not contribute to photo-current, see further). Likewise, cyclic current enhancements of the photodetectors under periodic illuminated and dark states at bias voltage of 1 V shown in **Figure 2c** shows better current enhancement of Ag@V_2O_5 photodetector as compared to other photodetectors. The slow dark current decays after switched off illumination of the photodetectors could be caused by oxygen vacancies related defects states.[31,32] The electrical measurements suggest that introduction of Ag with V_2O_5 enhance the overall photo-sensitivity as compared to the pristine counterpart. The absorbance (**Figure S4a**) and transmission spectra (**Figure 2d**) confirmed absorption of

light by SCNTs, MCNTs and Ag nanowires. Further, steady state photoluminescence (PL) (**Figure S4b**) and time resolved photoluminescence (TRPL) measurements (**Figure 2e**) are used to understand the photo-charge carrier dynamics of the photoanodes. **Figure 2e** shows the TRPL of the samples fitted using a bi-exponential time decay model.[33] Interestingly, the average charge carrier lifetime of the Ag@V_2O_5 significantly increased (~ 40%) as compared to that of pristine V_2O_5 counterpart. However, the carrier lifetimes of the SCNTs@V_2O_5 and MCNTs@V_2O_5 samples are decreased (~ 24% and ~ 23%) compared to that of V_2O_5. The observed enhancement in the steady state PL intensity and TRPL lifetime of Ag@V_2O_5 could be due to a combination of light scattering and potential defect passivation. Similar, bi-exponential or tri-exponential PL time decays associated with V_2O_5 systems have been observed earlier.[34,35]

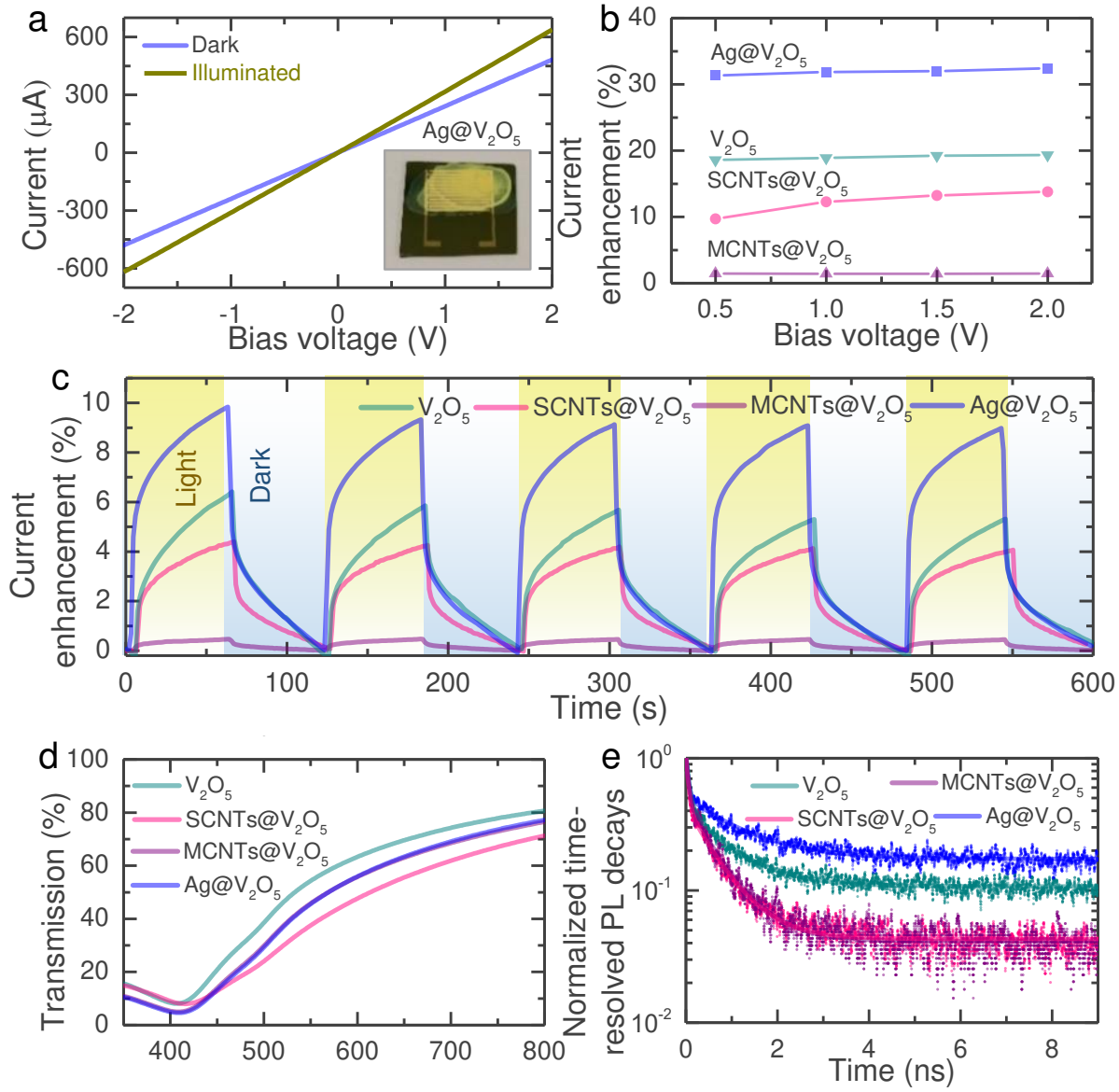

Figure 2. *(a) IV profiles of the Ag@V_2O_5 photodetector in dark and illuminated conditions (λ ~ 455 nm). (b) Current enhancements of the pristine V_2O_5, SCNTs@V_2O_5, MCNTs@V_2O_5 and Ag@V_2O_5 photodetectors at different bias voltages of 0.5 V, 1.0 V, 1.5 V and 2.0 V. (c) Cyclic current enhancements of the photodetectors under periodic illuminated and dark conditions at bias voltage of 1 V. (d) Transmission spectra of pristine V_2O_5, SCNTs@V_2O_5, MCNTs@V_2O_5 and Ag@V_2O_5 samples. (e) Time resolved PL decays of the V_2O_5, SCNTs@V_2O_5,*

MCNTs@V_2O_5 and Ag@V_2O_5 samples (407 nm pulsed excitation, repetition rate of 40MHz and fluence of 10 nJ cm^{-2} $pulse^{-1}$).

Next, photo-capacitors are prepared by drop casting a mixture of V_2O_5 and Ag nanowires, SWCNTs or MWCNTs on fluorine doped tin oxide (FTO) coated transparent glass substrates (see SEM images in **Figure S5a-d** and cross section SEM in **Figure S6**). These substrates are mounted in CR2450 coin cell, in which ~ 8 mm diameter hole are machined to allow for illumination of the anodes as depicted in **Figure S7a,b**. Zn strips were used to contact the FTO to the coin cell to allow efficient photo excited holes transportation (see **Figure S7b** and **Figure 1a**). Some Zn stripping and plating might take place on this strip, but based on the electrochemical analysis, the contribution of this process to the overall capacity is negligible. Then, the mass ratio of cathode (activated carbon (AC), **Figure S7c** shows SEM image) to photoanode was optimized to obtain the optimum cell capacity, which is found to be 1.3:1 as shown in **Figure S8**. Finally, we used glass microfiber separators and ~ 150 μL of 3 M $Zn(CF_3SO_3)_2$ aqueous electrolyte.

Cyclic voltammetry (CV) of the pristine V_2O_5, SCNTs@V_2O_5, MCNTs@V_2O_5 and Ag@V_2O_5 hν-ZICs was carried out in in dark and light conditions (λ ~ 455 nm, intensity ~ 12 mW cm^{-2}) to investigate the influence of light on the device current (see **Figure S9)**. The CVs of the Ag@V_2O_5 hν-ZIC at scan rates of 50 mV s^{-1}, 500 mV s^{-1} and 1000 mV s^{-1} are shown in **Figure 3a-c**. The capacity of the hν-ZICs increases when illuminated because the photo-generated charges contribute to the measured current, which increases with light intensity (**Figure 3d**). The highest capacity enhancement is observed in the Ag@V_2O_5 hν-ZIC as shown in **Figure 3e** which depicts capacity enhancements ($\frac{C_{ph}-C_d}{C_d} \times 100\%$; where C_d and C_{ph} are gravimetric capacities in dark and illuminated conditions). The capacity enhancement is ~ 35%, ~ 45%, ~

57%, and ~ 63% for MCNTs@V_2O_5, SCNTs@V_2O_5, pristine V_2O_5, and Ag@V_2O_5 hν-ZICs respectively (scan rate of 100 mV s^{-1}, λ ~ 455 nm, intensity ~ 12 mW cm^{-2}). In addition, CVs using different light wavelengths are shown in **Figure S10**.

The photo-charge mechanism of the Ag@V_2O_5 hν-ZIC can be explained from the energy band diagram of the photoanode shown in **Figure 1a**. We expect that the photo-excited holes move from the photoanode to the AC cathode through the external circuit because of the favorable energy pathways shown in **Figure 1a**, and the unpaired photo-excited electrons will accumulate on the photoanode. This process allows for diffusion of anions to the AC cathode to generate the electrical double layer capacitance and intercalation of cations in the photoanode for photo-charging. Hence, the addition of Ag nanowires to the photoanodes support photo-excited holes transport as well as provide light scattering centers to enhance the overall visible light absorption probabilities (**Figure 2d** and **S4a**). On the other hand, SWCNTs and MWCNTs do not offer favorable photo-excited holes transportation pathways because of energy levels mismatches at the interfaces (see energy band diagrams in **Figure S11**). Further, SWCNTs and MWCNTs absorb some light (as discussed earlier), which further decreases the capacity enhancement as shown in **Figure 3e**. The transport of photo-excited charge carriers through the external circuit is confirmed from the cyclic current response ($I_{ph} - I_d$ at 0 V applied voltage), which increases from 0 μA cm^{-2} to ~ 60 μA cm^{-2} under illumination (for 5 min) and returns to 0 μA cm^{-2} in dark states as shown in **Figure 3f**. These experiments were conducted using a new device which might have suffered from some degradation processes in the initial cycles contributing to the decrease in current observed in **Figure 3f**.

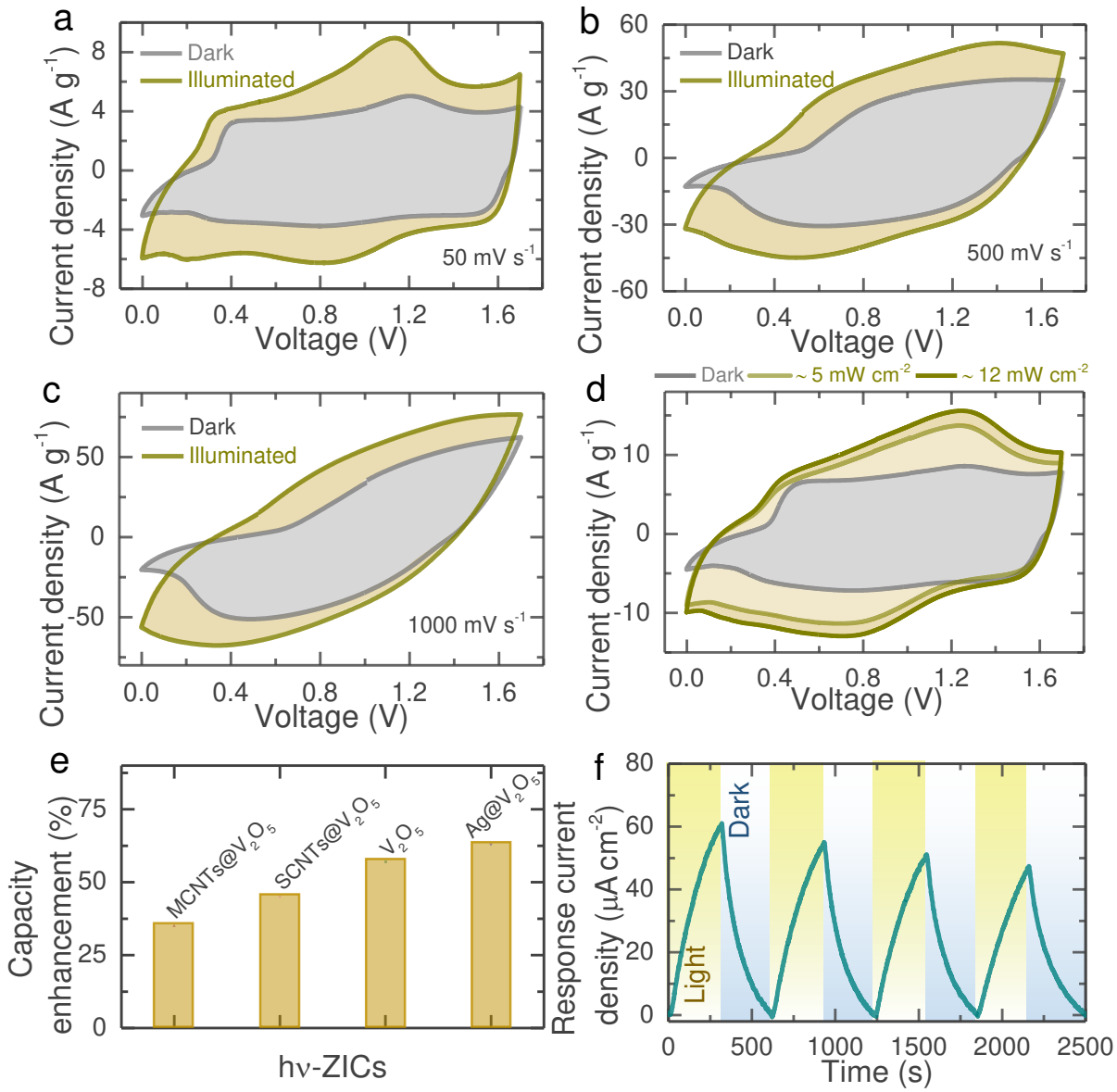

Figure 3. *(a-c) CV curves Ag@V_2O_5 hν-ZICs at scan rates of 50 mV s^{-1}, 500 mV s^{-1} and 1000 mV s^{-1} in dark and illuminated conditions (λ ~ 455 nm, intensity ~ 12 mW cm^{-2}). (d) CVs in dark and illuminated conditions (λ ~ 455 nm) at different light intensities of 5 mW cm^{-2} and 12 mW cm^{-2} at scan rate of 100 mV s^{-1}. (e) Comparative capacity enhancements of the pristine V_2O_5, SCNTs@V_2O_5, MCNTs@V_2O_5 and Ag@V_2O_5 hν-ZICs at scan rate of 100 mV s^{-1} under illumination (λ ~ 455 nm, intensity ~ 12 mW cm^{-2}). (f) Cyclic absolute response current of the Ag@V_2O_5 hν-ZIC in dark and light illuminated conditions at 0 V applied voltage.*

In what follows we investigate the electrochemical performance of Ag@V_2O_5 hν-ZICs in more detail. **Figure 4a,b** shows Galvanostatic charge-discharge (GCD) of Ag@V_2O_5 hν-ZICs both in dark and light (λ ~ 455 nm, intensity ~ 12 mW cm^{-2}), demonstrating clear capacity enhancements when illuminated (e.g. ~ 74% at 200 mA g^{-1} and ~ 51% at 500 mA g^{-1}). Lower current densities allow for longer light interaction and therefore show higher capacity enhancements as summarized in **Figure 4c**. **Figure S12a,b** show the enhancement in capacity and energy density as a function of the current density, which shows and increase in capacity over 40% even at high current densities of 2000 mA g^{-1}. Further, this value increases with increasing light intensity (**Figure S12c**). Finally, we calculate the energy density and power density of Ag@V_2O_5 hν-ZICs under illumination, which are ranging from 32.45 Wh kg^{-1} to 53.13 Wh kg^{-1} at 1384.61 W kg^{-1} to 36.74 W kg^{-1}. The Ragone plot in **Figure 4d** shows that in addition to offering light charging capabilities, the performance of this capacitor is comparable with state of the art asymmetric supercapacitors (AC vs metal oxides/hydroxides/sulfides electrodes).

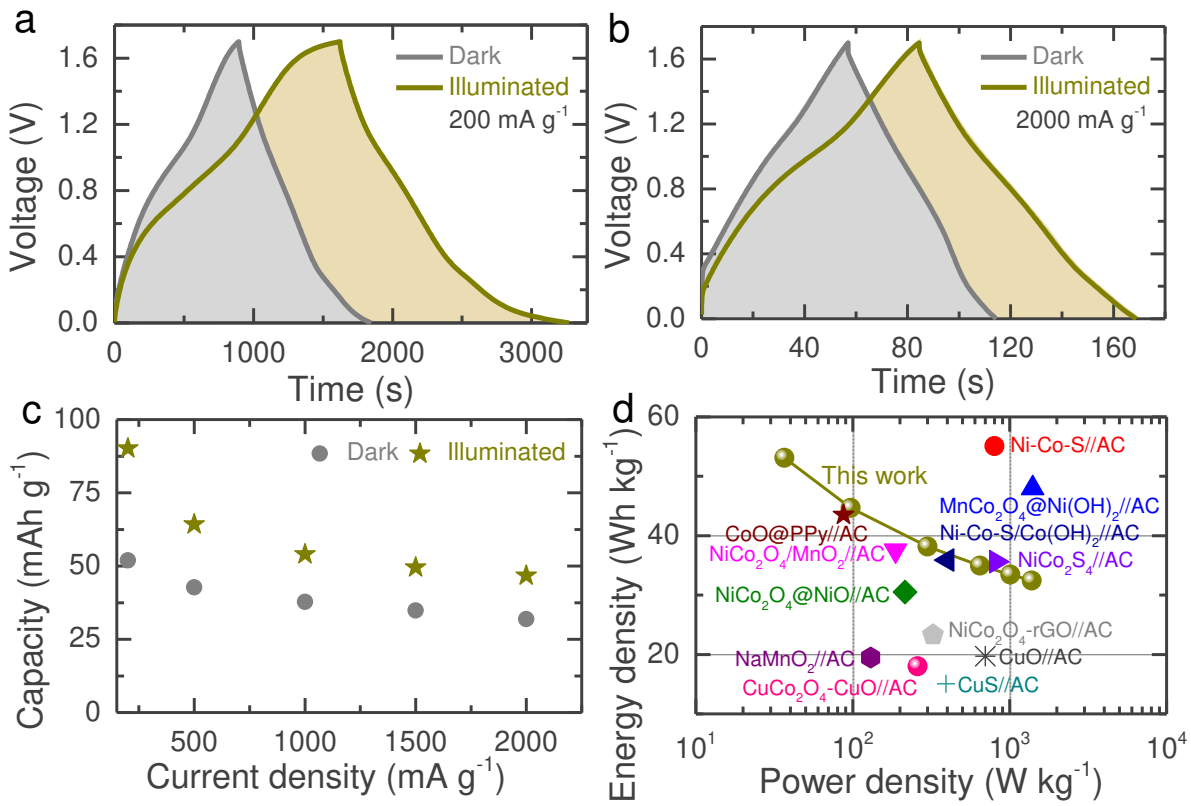

Figure 4. *(a,b) GCDs of the Ag@V_2O_5 hv-ZIC at current densities of 200 mA g^{-1} and 2000 mA g^{-1} in dark and illuminated (λ ~ 455 nm, intensity ~ 12 mW cm^{-2}) conditions. (c) Capacity with respect to current density plot of the Ag@V_2O_5 hv-ZIC in dark and illuminated. (d) Ragone plot shows the comparison of energy density and power density of our Ag@V_2O_5 hv-ZIC with those reported for asymmetric supercapacitors in literature: CuS//AC,[36] $CuCo_2O_4$-CuO//AC,[37] CuO//AC,[38] $NaMnO_2$//AC,[39] $NiCo_2O_4$-rGO//AC,[40] $NiCo_2O_4$@NiO//AC,[41] $NiCo_2O_4$/MnO_2//AC,[42] Ni-Co-S/$Co(OH)_2$//AC,[43] CoO@PPy//AC,[44] $NiCo_2S_4$//AC,[45] $MnCo_2O_4$@$Ni(OH)_2$//AC,[46] Ni-Co-S//AC,[47] etc .*

Impedance spectra in dark and illuminated conditions (λ ~ 455 nm, intensity ~ 12 mW cm^{-2}), in **Figure 5a** show that the series resistance of our Ag@V_2O_5 hv-ZICs remains similar when illuminated (decreases from ~ 2.9 Ω to ~ 2.35 Ω), whereas the charge transfer resistance decreases from ~ 25 Ω to ~ 9.5 Ω. This is in agreement with a reduction in impedance measured

in the I-V profiles of Ag@V_2O_5 when illuminated as shown in **Figure 2a**. The equivalent circuit of the Ag@V_2O_5 hν-ZICs in dark and illuminated conditions is shown in **Figure S13**. To study the long-term capacity retention of the Ag@V_2O_5 hν-ZIC, we measure CVs and GCDs for 500 cycles in dark and illuminated conditions. **Figure 5b** shows the 1st, 50th, 250th and 500th CV curve at a scan rate of 200 mV s^{-1} in illuminated conditions (λ ~ 455 nm, intensity ~ 12 mW cm^{-2}). There is no significant change in the CV profiles after 500 CV cycles. **Figure 5c,d** shows 4000 GCD cycles of the Ag@V_2O_5 hν-ZICs in dark and light conditions at a current density of 1000 mA g^{-1}. The Ag@V_2O_5 hν-ZICs achieve a capacity retention of ~ 99% after 4000 cycles in dark conditions and high coulombic efficiencies (~ 100% after 4000 cycles). When illuminated the capacity measured by GCD increases slightly over the 4000 cycles, which is probably related to the capacity increase seen in the CVs over time close to 0V (**Figure 5b**). These results further confirm the stability of the Ag@V_2O_5 hν-ZICs both in dark and illuminated conditions.

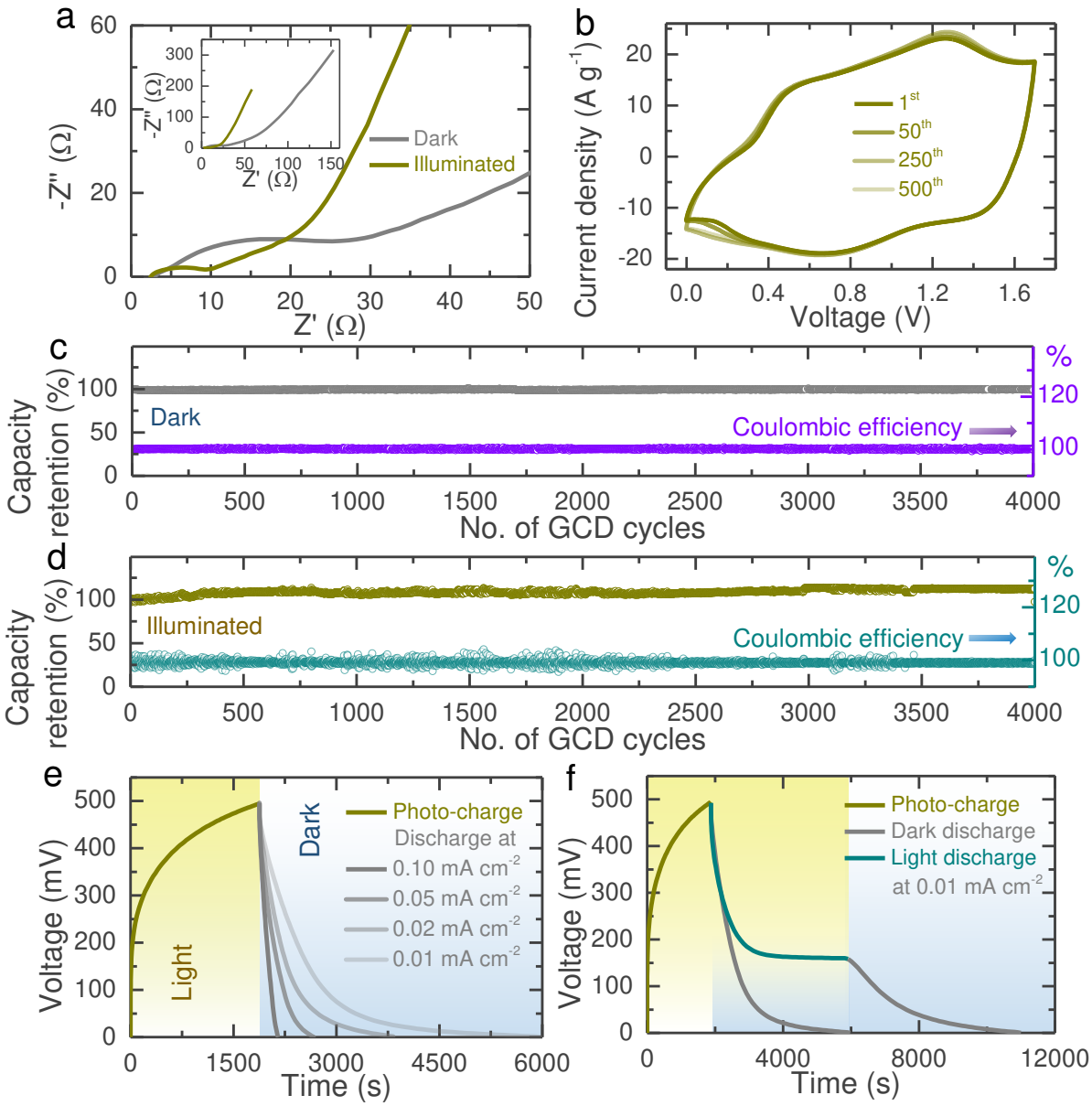

Figure 5. *(a) AC impedance of the Ag@V_2O_5 hv-ZIC in dark and illuminated conditions (λ ~ 455 nm, intensity ~ 12 mW cm^{-2}) acquired in the frequency range of 10 mHz to 100 kHz at amplitude of 10 mV. (b) 1st, 50th, 250th and 500th CV cycles of illuminated Ag@V_2O_5 hv-ZICs (λ ~ 455 nm, intensity ~ 12 mW cm^{-2}, scan rate of 200 mV s^{-1}) (c,d) Capacity retentions and coulombic efficiencies over 4000 GCD cycles at 1000 mA g^{-1} of the Ag@V_2O_5 hv-ZICs both in dark and light (λ ~ 455 nm, intensity ~ 12 mW cm^{-2}). (e) Photo-charge (λ ~ 455 nm, intensity ~ 12 mW cm^{-2}) and discharge at different current densities (0.1 to 0.01 mA cm^{-2}). (f) Discharges at 0.01 mA cm^{-2} in dark and illuminated conditions of photo-charged Ag@V_2O_5 hv-ZICs.*

The above experiments show how light influences CV and GCD curves, in what follows, we measure the charging of Ag@V_2O_5 hν-ZIC by light without applying any external current or voltage. **Figure 5e** shows the photo-charging curve, which takes about 30 min to reach 500 mV (λ ~ 455 nm, intensity ~ 12 mW cm^{-2}). At the discharge current densities of 0.1 mA cm^{-2} and 0.01 mA cm^{-2}, the measured photo-charged energy densities are ~1.67 μWh cm^{-2} at ~ 48 mF cm^{-2} and ~ 2.9 μWh cm^{-2} at ~ 83 mF cm^{-2}, respectively. The photo-charged hν-ZIC are then discharged at different current densities (**Figure 5e**). It is important to note that the Ag@V_2O_5 hν-ZIC can be charged by light while delivering a load as shown in **Figure 5f**. Photo-charged Ag@V_2O_5 hν-ZICs discharge slowler under illumination than in dark conditions, which is because the capacitor is recharged by light whilst at the same time being discharged galvanostatically. In these experiments, the device voltage output decreases until the current generated by the photo-charging process is equal to the discharge current. In the conditions used in this particular experiment, (discharge current density of 0.01 mA cm^{-2} and ~ 12 mW cm^{-2} illumination with λ ~ 455 nm), this equilibrium is reached at an output voltage of 160 mV (See **Figure 5f**). Once the light source is turned off, the Ag@V_2O_5 hν-ZIC discharges to 0 V as expected. Based on the photo-charging response, we calculate the photo conversion efficiency of our Ag@V_2O_5 hν-ZIC, which is ~ 0.05%. The photo conversion efficiency these hν-ZICs are nearly five times higher than that of the graphitic carbon nitride light rechargeable electrochemical capacitors. [25] In addition, The photo-charge energy density is improved from 0.7 to 4.8 Wh kg^{-1} and the capacity from 11.4 to 138 F g^{-1} compared to previous hν-ZICs.[25]

Overall, this report presents a photo-capacitor that can simultaneously harvest and store optical energy without the need of any solar cell or external circuitry. This is made possible by the internal photo-charge carriers' separation and transportation in our Ag@V_2O_5 electrodes. These devices outperform previously reported photo-capacitor, and achieve energy densities

of ~ 53 Wh kg^{-1} which is comparable to the best reported asymmetric supercapacitors. Finally, these devices achieve a capacity retention of 99% over 4000 cycles.

EXPERIMENTAL SECTION

Material Synthesis and Characterizations. V_2O_5 nanofibers were synthesized by a hydrothermal process.[26] First, 0.364 g V_2O_5 powder (Sigma-Aldrich) is mixed with 30 mL de-ionized water under stirring (~ 300 rpm) at room temperature for 30 min. Then, 5 mL of 30% H_2O_2 added into the solution and continued stirring for another 30 min. The resultant transparent orange solution was transferred into a ~ 40 mL autoclave and then placed in an oven to maintain at 205 ^oC for two days. The product was washed with de-ionized water and ethanol followed by alternative centrifugation and finally annealed at ~ 400 ^oC for 1 h in air. **Figure S14** shows SEM, EDS, XRD and Raman spectroscopy of the source material i.e. V_2O_5 powder used for the synthesis of V_2O_5 nanofibers.

The SCNTs, MCNTs and Ag nanowires are received from Sigma, Nanocyl and Sigma-Aldrich, which are used without further purification.

The samples were characterized by SEM (FEI Magellan 400L with an acceleration voltage of 5 kV), TEM equipped with an X-ray EDS (Talos F200X G2 with an acceleration voltage of 200 kV), XRD (Bruker D8 Advance, Cu Kα radiation), Raman spectroscopy (Renishaw InVia), and optical absorbance/transmission (PerkinElmer UV/VIS/NIR Spectrometer (Lamda 750)).

Preparation of Photo-electrodes. First, 94.8 mg V_2O_5 nanofibers and 0.2 mg Ag nanowires were dispersed in 2 mL N-Methyl-2-pyrrolidone (NMP, Sigma-Aldrich) using mixing (VWR Analog Vortex Mister) and ultra-sonication. Then, 5 mg polyvinylidene fluoride (PVDF, Solef 6020) binder added into solution to prepare the Ag@V_2O_5 electrode solution. Similarly, the other SCNTs@V_2O_5 and MCNTs@V_2O_5 electrode solutions are prepared by adding 0.2 mg SCNTs and 0.2 mg MCNTs with 94.8 mg V_2O_5 and 5 mg PVDF binder followed by same

procedure. Finally, the photoelectrodes are obtained by drop casting electrodes solutions on FTO coated glass substrates (received from Sigma-Aldrich, surface resistivity ~7 Ωsq^{-1}) followed by drying at ~ 120 ºC in vacuum oven.

Designing of hv-ZICs. The coin cell (CR2450) type hν-ZIC is designed followed by making a hole (~ 8 mm diameter) on coin cell for an optical window. The photoanode is placed on the optical window side and fixed using EPOXY (EVO-STIK) to allow for light illumination. The Zn strip (Alfa Aesar, 0.25 mm thick) was used for electrical connection between photoanode and coin cell. The Whatman glass microfiber filters paper separator is placed and added ~ 150 µL of 3 M $Zn(CF_3SO_3)_2$ (Sigma-Aldrich) aqueous electrolyte. Thereafter, the AC cathode is placed on top of the separator and finally assembled followed by placing the stainless steel disk and spacer.

Electrochemical Testing of the hv-ZICs. CVs at different scan rates and GCDs at different current densities in dark and illuminated conditions of the hν-ZICs are measured by using a Biologic VMP-3 galvanostat. Different light wavelengths of 455 nm, 470 nm, 528 nm, and white were used to test photo-charging response of the hν-ZICs. The AC impedance test of the *hv-ZIC* is measured in the frequency range (10 mHz to 100 kHz) in dark and illuminated (λ ~ 455 nm, intensity ~ 12 mW cm^{-2}). The photo-charge measurements of the hν-ZIC are acquired by measuring the open circuit voltage, and recorded the discharge responses at different applied current densities.

Fabrication of Photodetectors and Electrical Measurements. For electrical photoresponse measurements, the photodetectors are fabricated by direct drop casting V_2O_5, SCNTs@V_2O_5, MCNTs@V_2O_5 and Ag@V_2O_5 materials on Gold (Au, 40 nm)/Chromium (Cr, 10 nm) IDEs patterned on Si_3N_4/Si wafer followed by standard UV lithographic technique. The current-voltage responses of the photodetectors are recorded in voltage range (-2 V to +2 V) in dark

and illuminated (λ ~ 455 nm) using Agilent Sourcemeter integrated to Suss MicroTec Probe Station. Moreover, the cyclic current-time responses of the photodetectors are recorded under periodic light illumination at 1 V applied bias voltage.

Time Correlated Single Photon Counting. The carriers' lifetime of the sample was extracted using a biexponential decay model. The pulsed diode laser of 407 nm wavelength was used as an excitation source. The blue laser (407 nm) was driven using DH400, PicoQuant laser controller and generates pulses with 80 ps full width at half maximum (FWHM). This time-correlated single photon counting (TCSPC) setup encompasses of a monochromator coupled with a micro channel plate photomultiplier tube (MCP-PMT from Hamamatsu - R3809U-50) and TCSPC electronics (Lifespec-pc and VTC900 PC card from Edinburgh Instruments).

ASSOCIATED CONTENT

Supporting Information

The Supporting Information is available free of charge on the ACS Publications website

Raman of nanofibers (Figure S1), SEM images of SCNTs, MCNTs and Ag nanowires (Figure S2); IV profiles of the pristine V_2O_5, SCNTs@V_2O_5 and MCNTs@V_2O_5 photodetectors (Figure S3); Absorbance and steady state PL spectra of the samples (Figure S4); SEM images of the photoanodes (Figure S5); Cross-section SEM image (Figure S6); Digital photograph of optical coin cell and SEM image of AC (Figure S7); Capacity plot at different anode to cathode mass ratios (Figure S8); CV curves of the hν-ZICs in dark and illuminated (Figures S9 and S10); Energy band diagrams of the hν-ZICs (Figure S11); Capacity enhancement, energy density and capacity plots of the Ag@V_2O_5 hν-ZIC (Figure S12); Equivalent circuit of AC impedance results (Figure S13); SEM, EDS, Raman and XRD of the commercial V_2O_5 particles (Figure S14).

AUTHOR INFORMATION

Corresponding Authors

*E-mail: bd411@cam.ac.uk

mfld2@cam.ac.uk

Notes

The authors declare no competing financial interest.

ACKNOWLEDGEMENTS

The B. D. B. and M. D. V. acknowledge support from the Newton International Fellowship-Royal Society (UK) grant NIF\R1\181656. B. W. acknowledges support from the EPSRC Graphene CDT EP/L016087/1. S.N. acknowledges funding and support from a Royal Society-SERB Newton International Fellowship (NIF\R1\181365). S.D.S. acknowledges the Royal Society and Tata Group (UF150033) and the EPSRC (EP/R023980/1).

REFERENCES

1. Zeng, Q.; Lai, Y.; Jiang, L.; Liu, F.; Hao, X.; Wang, L.; Green, M. A. Integrated Photorechargeable Energy Storage System: Next-Generation Power Source Driving the Future. *Adv. Energy Mater.* **2020**, *10*, 1903930.

2. Gurung, A.; Qiao, Q. Solar Charging Batteries: Advances, Challenges, and Opportunities. *Joule*. **2018**, *2*, 1217.

3. Li, Q.; Liu, Y.; Guo, S.; Zhou, H. Solar Energy Storage in the Rechargeable Batteries. *Nano Today*. **2017**, *16*, 46.

4. Sun, Y.; Yan, X. Recent Advances in Dual-Functional Devices Integrating Solar Cells and Supercapacitors. *Sol. RRL* **2017**, 1700002.

5. Meng, H.; Pang, S.; Cui, G. Photo-Supercapacitors Based on Third-Generation Solar Cells. *ChemSusChem*. **2019**, *12*, 3431.

6. Hu, Y.; Bai, Y.; Luo, B.; Wang, S.; Hu, H.; Chen, P.; Lyu, M.; Shapter, J.; Rowan, A.; Wang, L. A Portable and Efficient Solar-Rechargeable Battery with Ultrafast Photo-Charge/Discharge Rate. *Adv. Energy Mater.* **2019**, *9*, 1900872.

7. Xu, J.; Chen, Y.; Dai, L. Efficiently Photo-Charging Lithium-Ion Battery by Perovskite Solar Cell. *Nat. Commun.* **2015,** *6*, 8103.

8. Liu, R.; Wang, J.; Sun, T.; Wang, M.; Wu, C.; Zou, H.; Song, T.; Zhang, X.; Lee, S. T.; Wang, Z. L.; Sun, B. Silicon nanowire/polymer hybrid solar cell-supercapacitor: a self-charging power unit with a total efficiency of 10.5%. *Nano Lett.* **2017**, *17*, 4240.

9. Vlad, A.; Singh, N.; Galande, C.; Ajayan, P. M. Design Considerations for Unconventional Electrochemical Energy Storage Architectures. *Adv. Energy Mater.* **2015**, *5*, 1402115.

10. Ahmad, S.; George, C.; Beesley, D. J.; Baumberg, J. J.; Volder, M. D. Photo-Rechargeable Organo-Halide Perovskite Batteries. *Nano Lett.* **2018**, *18*, 1856.

11. Um, H.-D.; Choi, K.-H.; Hwang, I.; Kim, S.-H.; Seo, K.; Lee, S.- Y. Monolithically integrated, photo-rechargeable portable power sources based on miniaturized Si solar cells and printed solid-state lithium-ion batteries. *Energy Environ. Sci.* **2017**, *10*, 931.

12. Chai, Z.; Zhang, N.; Sun, P.; Huang, Y.; Zhao, C.; Fan, H. J.; Fan, X.; Mai, W. Tailorable and Wearable Textile Devices for Solar Energy Harvesting and Simultaneous Storage. *ACS Nano* **2016**, *10*, 9201.

13. Ren, C.; Zhou, Q.; Jiang, W.; Li, J.; Guo, C.; Zhang, L.; Su, J. Investigation of Germanium Selenide Electrodes for the Integrated Photo-Rechargeable Battery. *Int. J. Energy Res.* **2020**, *44*, 6015.

14. Yin, Y.; Feng, K.; Liu, C.; Fan, S. A Polymer Supercapacitor Capable of Self-Charging under Light Illumination. *J. Phys. Chem. C* **2015**, *119*, 8488.

15. Boruah, B. D.; Misra, A. Voltage Generation in Optically Sensitive Supercapacitor for Enhanced Performance. *ACS Appl. Energy Mater.* **2019**, *2*, 278. doi.org/10.1021/acsaem.8b01248

16. Zhu, M.; Huang, Y.; Huang, Y.; Pei, Z.; Xue, Q.; Li, H.; Geng, H.; Zhi, C. Capacitance Enhancement in a Semiconductor Nanostructure-Based Supercapacitor by Solar Light and a Self-Powered Supercapacitor–Photodetector System. *Adv. Funct. Mater.* **2016**, *26*, 4481.

17. Boruah, B. D.; Mathieson, A.; Wen, B.; Feldmann, S.; Dose, W.; De Volder, M. Photo-rechargeable Zinc-ion Batteries. *Energy Environ. Sci.* **2020**, *13*, 2414.

18. Lou, S. N.; Sharma, N.; Goonetilleke, D.; Saputera, W. H.; Leoni, T. M.; Brockbank, P.; Lim, S.; Wang, D. –W.; Scott, J.; Amal, R.; Ng, Y. H. An Operando Mechanistic Evaluation of a Solar-Rechargeable Sodium-Ion Intercalation Battery. *Adv. Energy Mater.* **2017**, *7*, 1700545.

19. Ng, C.; Ng, Y. H.; Iwase, A.; Amal, R. Visible light-induced charge storage, on-demand release and self-photorechargeability of WO3 film. *Phys. Chem. Chem. Phys.* **2011**, *13*, 13421.

20. Zhang, Y. Z.; Wang, Y.; Cheng, T.; Yao, L. Q.; Li, X.; Lai, W. Y.; Huang, W. Printed

supercapacitors: materials, printing and applications. *Chem. Soc. Rev.* **2019**, *48*, 3229.

21. Wang, H.; Zhu, C.; Chao, D.; Yan, Q.; Fan, H. J. Nonaqueous Hybrid Lithium-Ion and Sodium-Ion Capacitors. *Adv. Mater.* **2017**, *29*, 1702093.

22. Ding, J.; Hu, W.; Paek, E.; Mitlin, D. Review of Hybrid Ion Capacitors: From Aqueous to Lithium to Sodium. *Chem. Rev.* **2018**, *118*, 6457.

23. Sun, G.; Yang, H.; Zhang, G.; Gao, J.; Jin, X.; Zhao, Y.; Jiang, L.; Qu, L. A Capacity Recoverable Zinc-Ion Micro-Supercapacitor. *Energy Environ. Sci.* **2018**, *11*, 3367.

24. Dong, L.; Ma, X.; Li, Y.; Zhao, L.; Liu, W.; Cheng, J.; Xu, C.; Li, B.; Yang, Q. H.; Kang, F. Extremely Safe, High-Rate and Ultralong-Life Zinc-Ion Hybrid Supercapacitors. *Energy Storage Mater.* **2018**, *13*, 96.

25. Boruah, B. D.; Mathieson, A.; Wen, B.; Jo, C.; Deschler, F.; De Volder, M. Photo-Rechargeable Zinc-Ion Capacitor using 2D Graphitic Carbon Nitride. *Nano Lett.* **2020**, *20*, 5967.

26. Zhai, T.; Liu, H.; Li, H.; Fang, X.; Liao, M.; Li, L.; Zhou, H.; Koide, Y.; Bando, Y.; Golberg, D. Centimeter-Long V2O5 Nanowires: From Synthesis to Field-Emission, Electrochemical, Electrical Transport, and Photoconductive Properties. *Adv. Mater.* **2010**, *22*, 2547.

27. Boruah, B. D.; Misra, A. ZnO Quantum Dots and Graphene Based Heterostructure for Excellent Photoelastic and Highly Sensitive Ultraviolet Photodetector. *RSC Adv.* **2015**, *5*, 90838. doi.org/10.1039/C5RA18663C

28. Dong, H.; Wu, Z.; Lu, F.; Gao, Y.; El-Shafei, A.; Jiao, B.; Ning, S.; Hou, X. Optics-

Electrics Highways: Plasmonic Silver Nanowires@TiO2 Core-Shell Nanocomposites for Enhanced Dye-Sensitized Solar Cells Performance. *Nano Energy* **2014**, *10*, 181.

29. Tan, H.; Santbergen, R.; Smets, A. H. M.; Zeman, M. Plasmonic Light Trapping in Thin-Film Silicon Solar Cells with Improved Self-Assembled Silver Nanoparticles. *Nano Lett.* **2012**, *12*, 4070.

30. Huang, J.; Chen, F.; Zhang, Q.; Zhan, Y.; Ma, D.; Xu, K.; Zhao, Y. 3D silver nanoparticles decorated zinc oxide/silicon heterostructured nanomace arrays as high-performance surface-enhanced Raman scattering substrates. *ACS Appl. Mater. Interfaces* **2015**, *7*, 5725.

31. Wu, J.; Ding, S.; Huang, Z.; Li, H.; Huang, K.; Qi, X.; Li, J. Improved photoresponse performances of V2O5 and rGO, *Fuller. Nanotub. Carbon Nanostructures* **2019**, *27*, 566.

32. Yalagala, B. P.; Sahatiya, P.; Kolli, C. S. R.; Khandelwal, S.; Mattela, V.; Badhulika, S. V2O5 Nanosheets for Flexible Memristors and Broadband Photodetectors. *ACS Appl. Nano Mater.* 2019, 2, 937.

33. Beura, R.; Pachaiappan, R.; Thangadurai, P. A Detailed Study on Sn 4+ Doped ZnO for Enhanced Photocatalytic Degradation. *Appl. Surf. Sci.* **2018**, *433*, 887.

34. Le, T. K.; Kang, M.; Han, S. W.; Kim, S. W. Highly Intense Room-Temperature Photoluminescence in V 2 O 5 Nanospheres. *RSC Adv.* **2018**, *8*, 41317.

35. Othonos, A.; Christofides, C.; Zervos, M. Ultrafast Transient Spectroscopy and Photoluminescence Properties of V 2O5 Nanowires. *Appl. Phys. Lett.* **2013**, *103*, 133112.

36. Zhang, J.; Feng, H.; Yang, J.; Qin, Q.; Fan, H.; Wei, C.; Zheng, W. Solvothermal Synthesis of Three-Dimensional Hierarchical CuS Microspheres from a Cu-Based Ionic Liquid Precursor for High-Performance Asymmetric Supercapacitors. *ACS Appl. Mater. Interfaces* **2015**, *7*, 21735.

37. Shanmugavani, A.; Selvan, R. K. Improved electrochemical performances of CuCo2O4/CuO nanocomposites for asymmetric supercapacitors. *Electrochim. Acta* **2016**, *188*, 852.

38. Moosavifard, S. E.; El-Kady, M. F.; Rahmanifar, M. S.; Kaner, R. B.; Mousavi, M. F. Designing 3D Highly Ordered Nanoporous CuO Electrodes for High-Performance symmetric Supercapacitors. *ACS Appl. Mater. Interfaces* **2015**, *7*, 4851.

39. Qu, Q. T.; Shi, Y.; Tian, S.; Chen, Y. H.; Wu, Y. P.; Holze, R. A New Cheap Asymmetric Aqueous Supercapacitor: Activated Carbon//NaMnO2. *J. Power Sources* **2009**, *194*, 1222.

40. Wang, X.; Liu, W. S.; Lu, X.; Lee, P. S. Dodecyl Sulfate-Induced Fast Faradic Process in Nickel Cobalt Oxide-Reduced Graphite Oxide Composite Material and Its Application for Asymmetric Supercapacitor Device. *J. Mater. Chem.* **2012**, *22*, 23114.

41. Liu, X.; Liu, J.; Sun, X. NiCo 2 O 4@ NiO hybrid arrays with improved electrochemical performance for pseudocapacitors. *J. Mater. Chem. A* **2015**, *3*, 13900.

42. Zhang, Y.; Wang, B.; Liu, F.; Cheng, J.; Zhang, X. wen; Zhang, L. Full Synergistic Contribution of Electrodeposited Three-Dimensional NiCo2O4@MnO2 Nanosheet Networks Electrode for Asymmetric Supercapacitors. *Nano Energy* **2016**, *27*, 627.

43. Li, R.; Wang, S.; Huang, Z.; Lu, F.; He, T. NiCo2S4@Co(OH)2 Core-Shell Nanotube Arrays in Situ Grown on Ni Foam for High Performances Asymmetric Supercapcitors. *J. Power Sources* **2016**, *312*, 156

44. Zhou, C.; Zhang, Y.; Li, Y.; Liu, J. Construction of High-Capacitance 3D CoO@Polypyrrole Nanowire Array Electrode for Aqueous Asymmetric Supercapacitor. *Nano Lett.* **2013**, *13*, 2078.

45. Wen, Y.; Peng, S.; Wang, Z.; Hao, J.; Qin, T.; Lu, S.; Zhang, J.; He, D.; Fan, X.; Cao, G. Facile Synthesis of Ultrathin NiCo2S4 Nano-Petals Inspired by Blooming Buds for High-Performance Supercapacitors. *J. Mater. Chem. A* **2017**, *5*, 7144.

46. Zhao, Y.; Hu, L.; Zhao, S.; Wu, L. Preparation of MnCo2O4@Ni(OH)2 Core–Shell Flowers for Asymmetric Supercapacitor Materials with Ultrahigh Specific Capacitance. *Adv. Funct. Mater.* **2016**, *26*, 4085.

47. He, W.; Liang, Z.; Ji, K.; Sun, Q.; Zhai, T.; Xu, X. Hierarchical Ni-Co-S@Ni-W-O Core–Shell Nanosheet Arrays on Nickel Foam for High-Performance Asymmetric Supercapacitors. *Nano Res.* **2018**, *11*, 1415.